Astrophysical constraints on non-standard coherent neutrino-nucleus scattering

Anna M. Suliga* and Irene Tamborra[†]
Niels Bohr International Academy and DARK, Niels Bohr Institute,
University of Copenhagen, Blegdamsvej 17, 2100, Copenhagen, Denmark
(Dated: June 14, 2022)

The exciting possibility of detecting supernova, solar, and atmospheric neutrinos with coherent neutrino-nucleus scattering detectors is within reach, opening up new avenues to probe New Physics. We explore the possibility of constraining non-standard coherent neutrino-nucleus scattering through astrophysical neutrinos. Sensitivity bounds on the mass and coupling of the new mediator are obtained by inspecting the modifications induced by the new interaction on the recoil rate observable in the upcoming RES-NOVA and DARWIN facilities. Under the assumption of optimal background tagging, the detection of neutrinos from a galactic supernova burst, or one-year exposure to solar and atmospheric neutrinos, will place the most stringent bounds for mediator couplings $g \gtrsim 10^{-5}$ and mediator masses between 1 and 100 MeV. A similar, but slightly improved, potential to CO-HERENT will be provided for larger mediator masses. In particular, RES-NOVA and DARWIN may potentially provide one order of magnitude tighter constraints than XENON1T on the mediator coupling. Non-standard coherent neutrino-nucleus scattering may also force neutrinos to be trapped in the supernova core; this argument allows to probe the region of the parameter space with $g \gtrsim 10^{-4}$, which is currently excluded by other coherent neutrino-nucleus scattering facilities.

I. INTRODUCTION

Coherent Elastic Neutrino-Nucleus Scattering ($\text{CE}\nu\text{NS}$) [1] has recently been observed by the COHERENT Collaboration [2, 3], despite the challenges due to the low recoil energy [4]. Such a measurement is of paramount importance to test standard physics, but above all, it opens new avenues to probe physics beyond the Standard Model (SM) [4–25].

Coherent Elastic Neutrino-Nucleus Scattering is also at the core of direct detection dark matter experiments, such as XENON1T [26], LUX [27], XMASS [28] and the upcoming XENONnT [29], LZ [30], and DARWIN [31]. The advantage of $CE\nu NS$ is the coherently enhanced cross section at low recoil energy coming from the square of the neutron number of the nucleus [32]. For this reason, the elastic scattering of neutrinos on protons or nuclei was proposed long ago as an attractive option to detect astrophysical neutrinos [33–35]. This detection technique would be complementary to existing dedicated astrophysical neutrino experiments [36, 37] and, being mediated through the Z boson, it would be flavor-insensitive.

Following up on this idea, Ref. [39] has highlighted the detection prospects of core-collapse supernova (SN) neutrinos in XENON1T and its future-generation extensions. In fact, typical SN neutrinos have an average energy of $\mathcal{O}(10)$ MeV, which would lead to a CE ν NS nuclear recoil of $\mathcal{O}(1)$ keV, in the range of interest of direct detection dark matter detectors based on Xenon (Xe) [40]. The transient nature of the SN burst and the high number of expected events would allow excellent detection perspectives, as also shown in Refs. [41, 42]. The detection of SN neutrinos through CE ν NS has also been explored

FIG. 1. Bounds on the new vector mediator coupling in the plane spanned by the vector mass $m_{Z'}$ and coupling g. Our new sensitivity bounds come from considering nonstandard neutrino-nucleus (nucleon) interactions in the SN core (marked by solid and dashed black lines), by detecting a neutrino burst from a galactic SN (green line and hatched region), as well as 1 yr exposure to solar and atmospheric neutrinos (orange line and hatched region) in DARWIN and RES-NOVA-3 (RN-3). Our prospective limits are contrasted with constraints from existing experiments (shaded regions): COHERENT [23] (light pink), SuperCDMS (beige), CDM-Slite (red), and LUX data (blue) [13]. The sensitivity of XENON1T has been calculated by relying on the limits provided in Ref. [38] (light green). DARWIN and RES-NOVA-3 have the potential to exclude the largest region of the parameter space. The bounds plotted here are for a vector mediator; similar ones can be derived for a scalar mediator (see main text for details).

in LZ [43], XMASS [44], and PICO-500 [45]. In addition, the fact that direct detection dark matter experi-

 $^{10^{-2}}$ SuperCDMS 10^{-3} 10^{-4} 10^{-5} 10^{-6} 10^{1} 10^{2} 10^{3} 10^{4} $m_{Z'}$ [MeV]

^{*} anna.suliga@nbi.ku.dk

[†] tamborra@nbi.ku.dk

ments are approaching the so-called neutrino floor [46–48] could also be exploited to detect solar [13, 49–51] and atmospheric neutrinos [52].

A new detector concept based on $\text{CE}\nu\text{NS}$ has been recently presented to hunt for astrophysical neutrinos: RES-NOVA [53]. The employment of an array of cryogenic detectors based on archaeological lead (Pb) and the high Pb cross section with the ultra-high radiopurity of archaeological Pb promise high event statistics in RES-NOVA with easy scalability to large detector volumes.

Building on these new exciting developments, in this work we aim at placing constraints on the light mediator of $\text{CE}\nu\text{NS}$ by adopting SN, solar, and atmospheric neutrinos. We exploit the effects that non-standard interactions could have both in the source and in the detector. In order to explore the largest region of the parameter space that could be eventually excluded, we focus on the perspective limits that could be set by the next-generation DARWIN [31] and RES-NOVA-3 [53], but also discuss the bounds potentially provided by XENONnT [29], and XENON1T [38].

Figure 1 displays the parameter space spanned by the new mediator coupling g and mass m excluded in this work by relying on the neutrino burst expected from a galactic SN, as well as solar and atmospheric neutrinos together with current limits from COHERENT [23], Super-CDMS, CDMSlite and LUX data [13, 54–56]. In addition, we have calculated the exclusion bounds for XENON1T [38]. Our work shows that the detection of SN neutrinos, or 1 yr exposure to solar and atmospheric neutrinos, would allow to probe the largest region of the parameter space spanned by the mass and coupling of the new mediator. Under the assumption of optimal background tagging and in the limit of low mediator mass, the potential improvement with respect to the limits from COHERENT [23], which are currently the most stringent ones, is up to 50%. In the near future new exciting possibilities of constraining non-standard mediators might come from the experiments focused on reactor neutrinos such as CONUS [57], ν -cleus [58], CONNIE [59], MINER [60], and RED [61]. In particular, CONUS is currently taking the data and its projected bounds in the new mediator parameter space may be competitive to the ones derived in this work [21, 22].

This paper is organized as follows. In Sec. II, a brief overview on coherent neutrino nucleus scattering is provided, and the cross section is generalized to include non-standard vector and scalar mediators. Section III introduces the expected recoil rate in DARWIN and RESNOVA. Section IV is centered on the impact of non-standard coherent neutrino nucleus scattering on the SN physics and on the detection of SN neutrinos. The effect of non-standard coherent neutrino nucleus scattering on the detection of solar and atmospheric neutrinos is shown in Secs. V and Sec. VI, respectively. The statistical analysis adopted to derive the bounds presented in Fig. 1 is outlined in Sec. VIII. Outlook and conclusions are presented in Sec. VIII. We explore the impact of the

uncertainty on the SN model on the sensitivity bounds in Appendix A, and the dependence of the SN neutrino rate on the mediator mass in Appendix B.

II. COHERENT NEUTRINO-NUCLEUS SCATTERING

Coherent Neutrino-Nucleus Scattering occurs between an active neutrino flavor and a nucleus

$$\nu + T(A, Z) \to \nu + T(A, Z) \tag{1}$$

where $A,\ Z$ are the atomic mass and number of the nucleus T. The differential $\text{CE}\nu\text{NS}$ cross section in the Standard Model is defined as [1]

$$\frac{d\sigma_{\rm SM}}{dE_r} = \frac{G_F^2 m_T}{4\pi} Q_w^2 \left(1 - \frac{m_T E_r}{2E_\nu^2} \right) F^2(Q) , \qquad (2)$$

where $m_T = 931.5 \text{ MeV} \times A$ is the target nucleus T mass, $Q_w = \left[N - Z(1 - 4\sin^2\theta_W)\right]$ is the weak vector nuclear charge, $\sin^2\theta_W = 0.231$ [62] the Weinberg angle, G_F is Fermi constant, E_R is the recoil energy of the nucleus T, E_{ν} the energy of a neutrino, and $Q = \sqrt{2m_T E_r}$ is the momentum transfer. The maximum recoil energy is $E_r^{\text{max}} = 2E_{\nu}^2/(m_T + 2E_{\nu})$. We employ the Helm-type form factor [45, 63]:

$$F(Q) = 3\frac{j_1(QR_0)}{QR_0} \exp{-\frac{1}{2}Q^2s^2} , \qquad (3)$$

with j_1 being the first order Bessel spherical function. The size of the nucleus T is equal to $R_0 = \sqrt{R^2 - 5s^2}$ with $R = 1.2A^{\frac{1}{3}}$, and the nuclear skin thickness is $s \approx 0.5$ fm [45]. In what follows, we modify Eq. 2 in order to take into account non-standard vector and scalar mediators.

A. New vector mediator

The Lagrangian term for the new vector mediator (Z') coupling to neutrinos and quarks reads

$$\mathcal{L}^{Z'} = g_{\nu,Z'} Z'_{\mu} \bar{\nu}_L \gamma^{\mu} \nu_L + Z'_{\mu} \bar{q} \gamma^{\mu} g_{q,Z'} q . \tag{4}$$

In this case the cross section in Eq. 2 is modified as follows [13, 23]

$$\frac{d\sigma_{\nu N}}{dE_r} = \frac{G_F^2 m_T}{\pi} |\xi|^2 \left(1 - \frac{m_T E_r}{2E_{\nu}^2} \right) F^2(Q) , \qquad (5)$$

where

$$\xi = -\frac{Q_w}{2} + \frac{g_{\nu,Z'}Q_w'}{\sqrt{2}G_F(2m_T + m_{Z'}^2)} \ . \tag{6}$$

In our framework we assume that the couplings to all quarks, $g_{q,Z'}$, are such that $Q'_w = g_{q,Z'}3A$ [13].

B. New scalar mediator

For a scalar mediator (ϕ) , the new Lagrangian term is

$$\mathcal{L}^{\phi} = g_{\nu,\phi}\phi\bar{\nu}_R\nu_L + \phi\bar{q}g_{q,\phi}q \tag{7}$$

for the lepton number conserving (LNC) coupling. Analogously, the lepton number violating (LNV) Lagrangian term is

$$\mathcal{L}^{\phi} = g_{\nu,\phi} \phi \nu_L^c \nu_L + \phi \bar{q} g_{q,\phi} q . \tag{8}$$

Note that, due to the chirality-flipping nature of the new interaction (for both LNC and LNV couplings), the scattering may be no longer elastic as the outgoing neutrino may have opposite handness, which means that a sterile neutrino may be produced in the LNC case and antineutrino in the LNV case. Hence, in the following, we will use $C\nu NS$ (instead than $CE\nu NS$) when dealing with the scalar mediator.

The total cross section in the presence of the new scalar mediator is [21, 23]:

$$\frac{d\sigma_{\nu N}}{dE_r} = \frac{d\sigma_{\rm SM}}{dE_r} + \frac{d\sigma_{\phi}}{dE_r} , \qquad (9)$$

where $d\sigma_{\rm SM}(E_{\nu})/dE_r$ is defined as in Eq. 2 and the term related to the new mediator is [21, 23]

$$\frac{d\sigma_{\phi}}{dE_r} = \frac{(g_{\nu,\phi}g_{q,\phi}Q_s)^2}{2\pi(2E_rm_T + m_{\phi}^2)^2} \frac{m_T^2 E_r}{2E_{\nu}^2} F^2(Q) , \qquad (10)$$

with $Q_s = \sum_{N,q} m_N/m_q f_{T_q}^N \approx 14A + 1.1Z$; the hadronic form factors $f_{T_q}^N$ follow the ones used in Ref. [13]. Throughout the paper, if not otherwise specified, we always assume $g = \sqrt{|g_{q,i}g_{\nu,i}|}$, where $g_{q,i}g_{\nu,i} > 0$ and $i = \{Z', \phi\}$.

III. EVENT RATES IN RES-NOVA AND DARWIN

The interaction of astrophysical neutrinos through $CE\nu NS$ (and $C\nu NS$ for a scalar mediator, see Sec. II B) in the detector, in the presence of non-standard interactions, is described by the following differential rate:

$$\frac{dR_{\nu N}}{dE_r dt} = N_T \, \epsilon(E_r)
\times \int dE_{\nu} \, \frac{d\sigma_{\nu N}}{dE_r} \, \psi(E_{\nu}, t) \, \Theta(E_r^{\text{max}} - E_r) ,$$
(11)

where N_T is the number of target nuclei in the detector volume, $\epsilon(E_r)$ is the detector efficiency, $\psi(E_{\nu})$ is the neutrino flux, Θ is the Heaviside step function, and E_r^{max} is defined as in Sec. II.

In this work, we mainly focus on RES-NOVA and DARWIN, which are the largest upcoming detectors employing CE ν NS. In order to estimate the effect of non-standard CE ν NS (and C ν NS) occurring in the detector,

we explore the effects induced on the recoil rate by non-standard interactions of astrophysical neutrinos in Pb and Xe detector in Secs. IV–VI by relying on the scattering rates per ton-year per target material. We will then apply our findings to RES-NOVA and DARWIN in Sec. VII. In the following, we introduce the general features of these detectors.

A. RES-NOVA

RES-NOVA is a proposed cryogenic detector to be likely installed at the Gran Sasso National Laboratories [53]. The sensitive detector component should be made of archaeological Pb. The ultra-low radioactivity of archaeological Pb and the largest $\text{CE}\nu\text{NS}$ cross section of Pb, among the stable elements, have the potential to guarantee high statistics.

Unless otherwise specified, we assume a detector effective volume of 456 ton (corresponding to RES-NOVA-3, planned after the first two extensions: RES-NOVA-1,2), 100% detection efficiency, and 1 keV recoil energy threshold. We refer the reader to Ref. [53] for more details.

In what follows, we assume negligible backgrounds in RES-NOVA. The irreducible detector background, originating from the decay of radioactive isotopes, is neglected; this assumption is justified for the detection of SN neutrinos, since the background rate of archeological Pb is several orders of magnitude lower than the SN signal rate. In the case of atmospheric and solar neutrinos, this background can be reduced significantly by relying on particle identification techniques [53]. In addition, an efficient suppression of the cosmogenic neutron background can also be achieved [53].

B. DARWIN

Dual-phase Xe detectors are sensitive to sub-keV nuclear recoil energies, with very low background and excellent time resolution. The detection of the prompt scintillation light (the S1 signal) from the liquid phase of the detector and the delayed scintillation photons (the S2 signal), caused by the drifting ionization electrons in the gaseous phase of the detector, allows for disentangling the electronic and nuclear recoils based on the S2/S1 ratio. DARWIN is expected to succeed XENON1T, and XENONnT at Gran Sasso National Laboratories.

DARWIN will have an effective volume of 40 ton. The detector efficiency is estimated to be between 100% and the energy-dependent one shown in Fig. 1 of Ref. [38, 64]; the energy threshold is of 1 keV [31] (see Refs. [31, 38, 64] for more details).

Similarly to RES-NOVA, the irreducible detector backgrounds for neutrino detection in DARWIN are arising from cosmogenic neutrons and the radioactivity of the intrinsic detector materials. Again, these backgrounds can be safely neglected for the study of SN neutrinos [39].

For the detection of solar and atmospheric neutrinos, the cosmogenic background in DARWIN can be eliminated to a very good extent by means of an active veto, self-shielding, and by rejection of multiple scattering events [31]. The low radioactivity of the detector material will be achieved with purification techniques and rejection techniques based on looking at the S2 to S1 signal ratio [31].

Ours is an exploratory study where we aim at comparing the sensitivity to New Physics of RES-NOVA and DARWIN. Hence, we refrain from estimating the S1 and S2 signals detectable in DARWIN and focus on the nuclear recoil event rates. It should also be noted that the distinction between the nuclear and electronic recoils has already been achieved in XENON1T [38, 64] and its predecessors.

IV. SUPERNOVA NEUTRINOS

Core-collapse SNe are among the densest neutrino sources [65, 66]. In this section, we first place constraints on non-standard neutrino nucleon coherent scattering in the source and then focus on the non-standard interactions of SN neutrinos occurring in the detector.

A. Non-standard coherent scattering in the supernova core

In the SN core, the matter density is large enough $[\rho \simeq \mathcal{O}(10^{14}) \text{ g cm}^{-3}]$ that neutrinos are trapped. If neutrinos undergo non-standard coherent scattering with the nucleons, for large enough couplings, they could be trapped for too long in the SN core, and hence fail in reviving the shock, according to the delayed neutrino-driven explosion mechanism [67].

In order to estimate the diffusion time of neutrinos, first we calculate the mean distance that a neutrino can travel between interactions, i.e., the average mean-free path:

$$\lambda_{\nu_{\beta}} = \sum_{\text{CC,NC}} \frac{\int dE_{\nu_{\beta}} f(E_{\nu_{\beta}}) E_{\nu_{\beta}}^2}{n_t \int dE_{\nu_{\beta}} f(E_{\nu_{\beta}}) E_{\nu_{\beta}}^2 \sigma_i(E_{\nu_{\beta}})} , \qquad (12)$$

where $f(E_{\nu_{\beta}})$ is the Fermi-Dirac distribution for the β -flavor (anti)neutrino, n_t is the number of targets for charged-current (CC) or neutral current (NC) interactions. Given that we focus on nuclear densities, we assume that the scattering on nucleons is the driving contribution in determining the mean-free path $(\nu_e + n \rightarrow e^- + p, \ \bar{\nu}_e + p \rightarrow e^+ + n, \ \text{and} \ \nu_{\beta} + N \rightarrow \nu_{\beta} + N)$. The CC cross sections have been implemented following Ref. [68]. The standard and non-standard NC scattering on neutrons [protons] have been estimated by replacing $Q_w \rightarrow 1 + 3g_A \ [(1 - 4\sin^2\theta_W) + 3g_A] \ [69]$ in Eqs. 2, 10 and 5 and assuming $F(Q^2) \approx 1$.

The diffusion time of neutrinos is

$$\tau_{\nu_{\beta}} = \int_{R_1}^{R_2} dr \frac{r}{\lambda_{\nu_{\beta}}(r)} , \qquad (13)$$

where R_1 defines the inner boundary where neutrino degeneracy becomes negligible and Pauli blocking is not large anymore, and R_2 stands for the outer radius where neutrinos start to free stream. In the following, we focus on electron neutrinos and antineutrinos as they are mainly responsible for depositing energy to revive the stalled shock [66]. To estimate the diffusion time, we rely on a time snapshot ($t_{\rm pb}=0.25~{\rm s}$) from a one-dimensional spherically symmetric SN simulation with $18.6~M_{\odot}$ mass [70] and SFHo [71] nuclear equation of state. Note that these inputs should be considered as indicative in order to gauge the impact of non-standard coherent scattering and do not qualitatively affect our findings.

Figure 2 shows a contour plot of the average diffusion time of (anti)neutrinos in the plane spanned by m and g, for the vector (scalar) mediator on the left (right). The average diffusion time is defined as $\tau = 1/2(\tau_{\nu_e} + \tau_{\bar{\nu}_e})$, and it is the time required for electron neutrinos and antineutrinos to travel between $R_1=10~\mathrm{km}$ and $R_2=40~\mathrm{km}$. We have chosen R_1 such that the degeneracy parameter $\eta = \mu/T = 1$ (with μ and T being the ν_e chemical potential and medium temperature, respectively) and hence Pauli blocking is negligible; R_2 coincides with the neutrinosphere (i.e., the surface above which neutrinos free stream). In the presence of non-standard coherent scattering, we exclude the region of the parameter space such that $\tau \gtrsim 10~(100)$ s. In this circumstance, neutrinos will be trapped for too long, possibly halting the shock revival, and this would be in conflict with the neutrino signal observed from SN 1987A [72, 73].

The region of the parameter space where the new mediator coupling highly affects the diffusion time of neutrinos, making it longer than $\tau=10~(100)$ s, lays above the black dashed (solid) lines in Fig. 2. The excluded region is smaller for the vector mediator case because of the presence of the interference term in the cross section (Eq. 6) that reduces the NC contribution to the diffusion time when the standard coupling is comparable to the non-standard one.

The scalar mediator case is more complex. In fact, the diffusion time criterion is applicable both for LNC and LNV couplings. However, for LNV coupling, neutrinos can convert to antineutrinos. As a result, the new interactions can have a drastic impact on the protoneutron star evolution [21] and, possibly, on neutrino flavor conversions eventually occurring before neutrino decoupling [74]. However, a self-consistent modeling of these effects is out of reach at the moment and it is beyond the scope of this paper.

For the LNC scalar mediator, left-handed neutrinos convert to right-handed ones (effectively becoming steriles). In this case, the total number of neutrino-nucleon

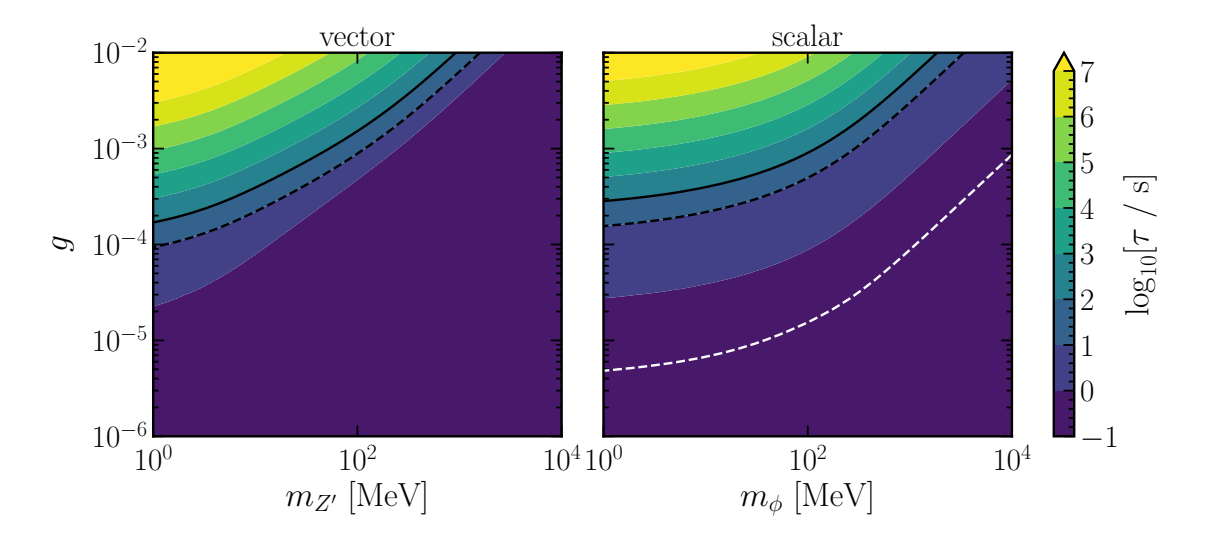


FIG. 2. Contour plot of the average diffusion time of neutrinos in the SN core in the $(g, m_{Z'} [g, m_{\phi}])$ parameter space for the vector [scalar] mediator on the left [right]. The black lines mark the average diffusion time $\tau = 10$ s (dashed) and 100 s (solid); see text for details. For the LNC scalar mediator we also show the white (grey) line above which ν_e (ν_x) are expected to scatter on nucleons at least once (cooling argument, see text). The regions of the parameter space above the black and white curves are excluded.

scatterings according to the central limit theorem [75] is

$$N = \int_0^{R_2} \frac{2r}{\lambda(r)^2} \, dr \ . \tag{14}$$

If all neutrinos, on average, scatter once before reaching the neutrinosphere (R_2) , it means that they are converted to right-handed particles. As such, there should be an extra cooling channel [76] that would shorten the timescale of the neutrino signal otherwise observed from the SN 1987A or even cause it to disappear. Hence, in the right panel of Fig. 2, we exclude the region of the parameter space such that $N \gtrsim 1$. This argument excludes a bigger fraction of the (g, m_{ϕ}) parameter space than the diffusion argument.

Despite the fact that we rely on inputs from one hydrodynamical SN simulation and develop detailed calculations of the neutrino mean-free path, diffusion time, and number of neutrino-nucleon interactions, our findings are in good agreement with the ones of Ref. [21]. In Ref. [21] the authors estimated the bounds on the mediator mass and coupling for a constant matter density and a single neutrino energy, using our same arguments.

B. Non-standard coherent scattering of supernova neutrinos in the detector

In order to estimate the event rate of SN neutrinos expected in RES-NOVA and DARWIN, we rely on the outputs of two one-dimensional spherically symmetric corecollapse SN models [70]. Since core-collapse SNe may be as likely as black hole forming collapses [77, 78], we adopt a core-collapse SN model with $27~M_{\odot}$ (CC-SN)

and a 40 M_{\odot} black-hole-forming collapse model (failed SN) as inputs for our computations. The neutrinos emitted during the SN burst have a pinched thermal energy distribution [79, 80]

$$\phi_{\nu_{\beta}}(E_{\nu_{\beta}}, t_{\rm pb}) = \xi_{\nu_{\beta}}(t_{\rm pb}) \left(\frac{E_{\nu_{\beta}}}{\langle E_{\nu_{\beta}}(t_{\rm pb})\rangle}\right)^{\alpha_{\beta}(t_{\rm pb})} \times \exp\left[-\frac{(1 + \alpha_{\beta}(t_{\rm pb}))E_{\nu_{\beta}}}{\langle E_{\nu_{\beta}}(t_{\rm pb})\rangle}\right],$$
(15)

where the pinching factor is given by

$$\alpha_{\beta}(t_{\rm pb}) = \frac{2\langle E_{\nu_{\beta}}(t_{\rm pb})\rangle^2 - \langle E_{\nu_{\beta}}(t_{\rm pb})^2\rangle}{\langle E_{\nu_{\beta}}(t_{\rm pb})^2\rangle - \langle E_{\nu_{\beta}}(t_{\rm pb})\rangle^2} \ . \tag{16}$$

The time-integrated neutrino flux is calculated as

$$\psi(E_{\nu_{\beta}}) = \int_0^{t_{\text{max}}} dt_{\text{pb}} \, \frac{L(t_{\text{pb}})}{4\pi D^2} \frac{\phi_{\nu_{\beta}}(E_{\nu_{\beta}}, t_{\text{pb}})}{\langle E_{\nu_{\beta}}(t_{\text{pb}}) \rangle} , \qquad (17)$$

where D is the SN distance from Earth; in the following, we consider $t_{\rm max}=14$ s and $t_{\rm max}=0.2$ s for the CC-SN and failed SN respectively, and D=10 kpc unless otherwise stated. Since the CE ν NS (C ν NS) interaction is not flavor sensitive, we do not worry about neutrino flavor conversions and consider the total neutrino flux summed over six flavors.

Figure 3 illustrates the event rate of SN neutrinos for Pb based (orange color) and Xe based (green lines) detectors for standard (solid lines) and non-standard interactions (non-solid lines) for the CC-SN [failed SN] on the top [bottom] panels. The number of events of the black-hole-forming collapse at high recoil energies (above the detection threshold) exceeds the number of events from

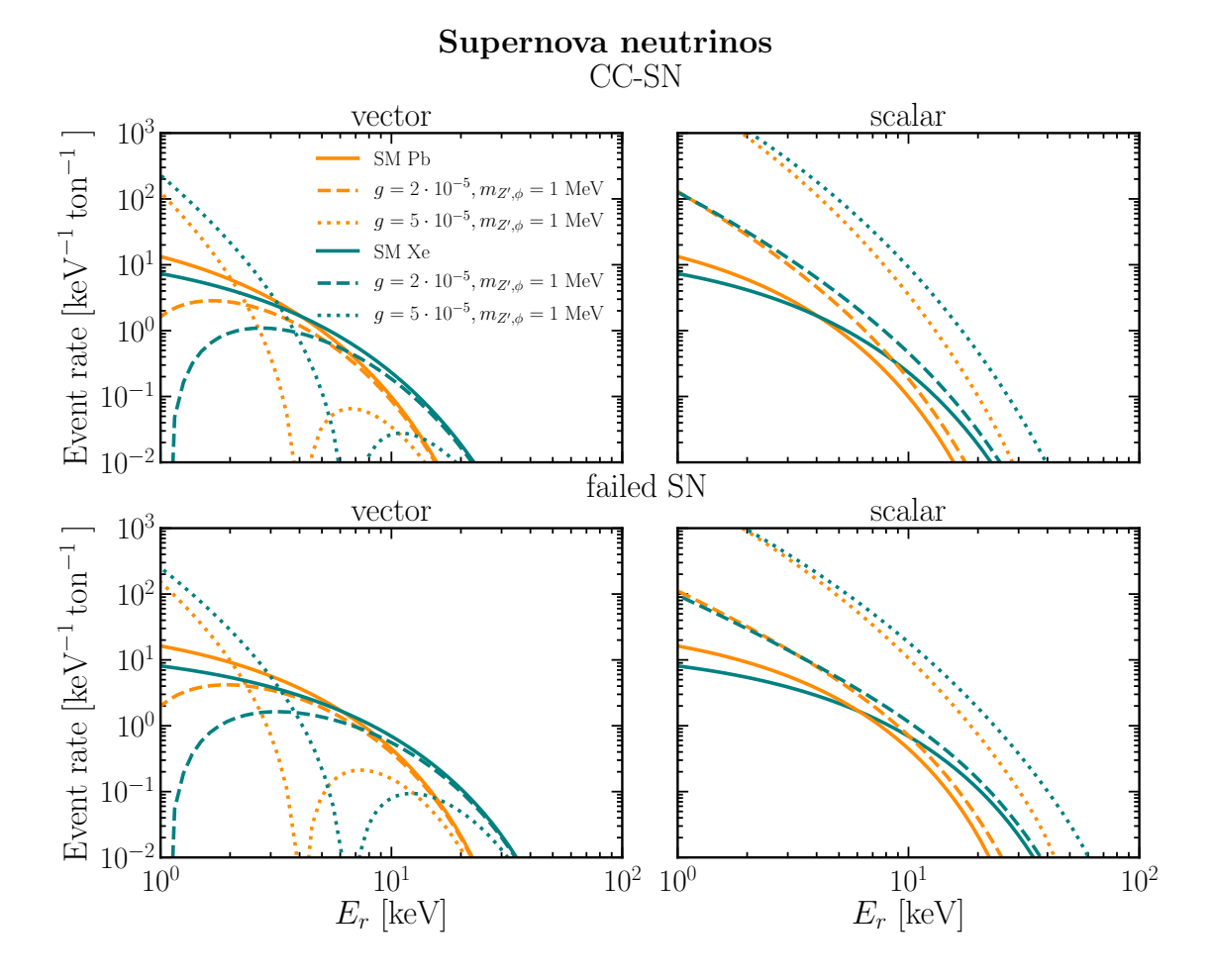


FIG. 3. Expected event rate as a function of the nuclear recoil energy for a CC-SN (top panels) and a failed SN (bottom panels) at 10 kpc from Earth in Pb (orange curves) and Xe (blue curves) based detectors. The standard event rates (solid lines) are shown together with the non-standard rates for vector and scalar mediators, on the left and right panels, respectively. The scalar mediator only increases the event rate with respect to the standard case; this is not true for the vector mediator case.

the core-collapse SN. This is because of the hotter neutrino spectra emitted in black-hole-forming collapses [66]. The Pb based detector is characterized by a total number of events above threshold (1 keV) higher than the Xe one; this is due to the fact that the event rate scales as the number of neutrons of the target. However, due to the heavier target, the range of observed recoil energies is smaller for Pb.

The left (right) panels of Fig. 3 illustrate the modifications in the expected event rate for different values of g and $m_{Z',\phi}=1$ MeV. The number of events as a function of the recoil energy for the new scalar interaction increases with respect to the standard case. In contrast, the event rate can be smaller than in the standard case for the vector mediator scenario. This can be easily understood by comparing the total cross sections for scalar (Eq. 10) and vector (Eq. 5) mediators. In the fist case, the cross section can only increase, if the quark and neutrino couplings to the new mediator are positive. Yet, for the vector mediator, the total cross section is the sum of

the contributions from the new vector mediator and the Z boson; hence, the interference term between these two can lead to a depletion of the event rate when the interference term dominates.

V. SOLAR NEUTRINOS

The sun is the closest astrophysical source of neutrinos, see Ref. [65] for a recent overview and references therein. Solar neutrinos are very useful to constrain nonstandard scenarios, see e.g. Refs. [13, 46, 48, 50, 81–84]. In principle, bounds on light mediators coupling to neutrinos and quarks may be derived by looking at neutrino interactions with the nucleons inside the sun. However, the solar density $[\rho \simeq \mathcal{O}(10-100) \text{ g/cm}^{-3}]$ is too low to trap neutrinos even for large g, hence the non-standard coherent neutrino-nucleus scattering affects the physics of the sun negligibly, differently from what discussed in the SN case in Sec. IV A.

Solar neutrinos

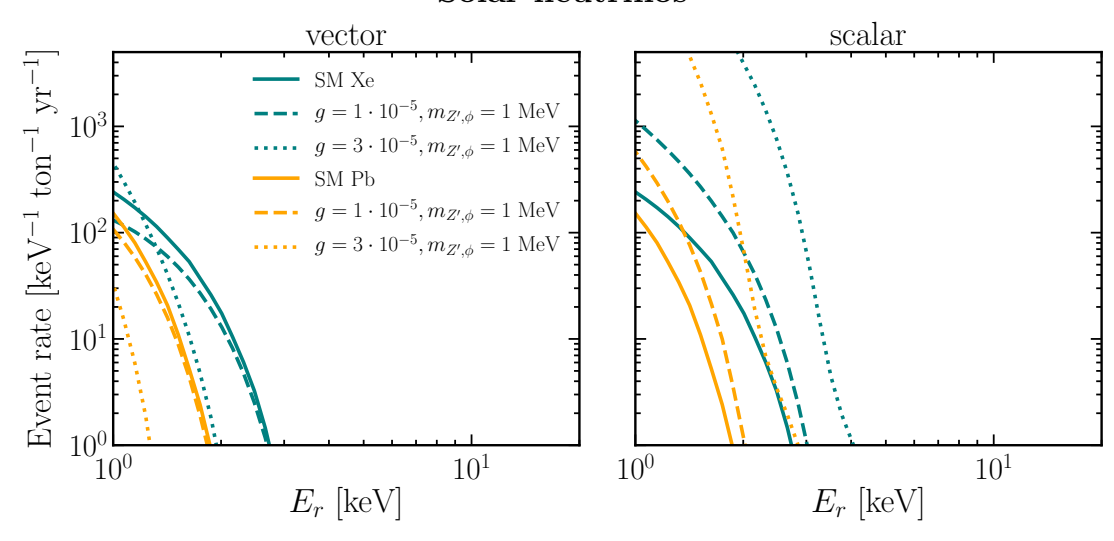


FIG. 4. Expected event rate as a function of the nuclear recoil energy induced by solar neutrinos in Pb (orange) and Xe (blue) based detectors. The standard event rate (solid line) is shown together with the non-standard one for the vector and scalar mediator on the left and right panels, respectively. The Xe based detector has an advantage over the Pb based detector thanks to the recoil spectrum extending to higher energies.

The detection of solar neutrinos in Pb and Xe based detectors could, however, allow one to constrain non-standard coherent neutrino nucleus scattering. This option is especially interesting since, as we approach the neutrino floor in direct detection dark matter experiments, the detection of solar neutrinos is within reach [13, 46]. In order to estimate the event rate of solar neutrinos, we consider the flux of neutrinos coming from two nuclear processes in the Sun

$$^{8}\text{B} \to {}^{8}\text{Be}^{*} + e^{+} + \nu_{e}$$
 (18)

and

$${}^{3}\text{He} + p \rightarrow {}^{4}\text{He} + e^{+} + \nu_{e} \ .$$
 (19)

These reactions produce neutrinos with energy up to 15 MeV. The rest of the neutrinos made in the pp and CNO chains, that fuel the sun, create neutrinos with typical energies that are too low to produce nuclear recoils above the 1 keV threshold. The solar neutrino fluxes adopted in this work were obtained by averaging the lower and upper bounds provided in the tables of Ref. [65].

The expected rate of solar neutrinos is shown in Fig. 4 for Xe and Pb targets for the standard case (solid lines). Similarly to the SN event rate (Fig. 3), the recoil spectrum ends at a smaller recoil energy for the Pb detector because the maximum recoil energy $(E_r^{\rm max})$ is smaller for a heavier detector material. Yet, due to the fact that the maximum neutrino energy produced by the nuclear reactions in the sun ($\sim 15~{\rm MeV}$) is much smaller than in the SN case ($\sim 50~{\rm MeV}$), we can see that the expected recoil energies produced by solar neutrinos lay below 5 keV.

For the same reason, the crossing between the event rates of the Xe and Pb based detectors lays below the 1 keV threshold, causing the Xe rate to be higher than the Pb one in the plotted energy range.

The impact of a non-standard mediator with 1 MeV mass in the interactions of solar neutrinos with the detector targets is displayed in Fig. 4 for different couplings g, on the left for the vector mediator and on the right for the scalar one. In both cases, the event rate is shown for Xe and Pb targets. The maximum recoil energy in the case of the Xe based detector is almost twice the one of the Pb detector; this allows to look for energy-dependent features in the recoil spectra over a broader range of energies in Xe based detectors. As we will discuss in Sec. VII, this opportunity helps to constrain the vector mediator at low and intermediate masses (see Fig. 8). This is not as important for the scalar mediator because in the low mediator mass limit the non-standard cross section (Eq. 9) does not depend on the mediator mass nor on the target mass. One can also notice that the event rate for the scalar mediator is always increasing with respect to the standard one, contrarily to the vector case, as dictated by the cross sections in Eqs. 5 and 9. In addition, for the same coupling, the difference between the standard and non-standard event rate is bigger for the scalar mediator in the low mass limit, due to the lack of neutrinos with energies higher than ~ 15 MeV and the $E_r^{-1}E_{\nu}^{-2}/2$ dependence of the scalar cross section as opposed to $(1 - m_T E_r E_{\nu}^{-2}/2)$ in the interference term of vector cross section.

Atmospheric neutrinos

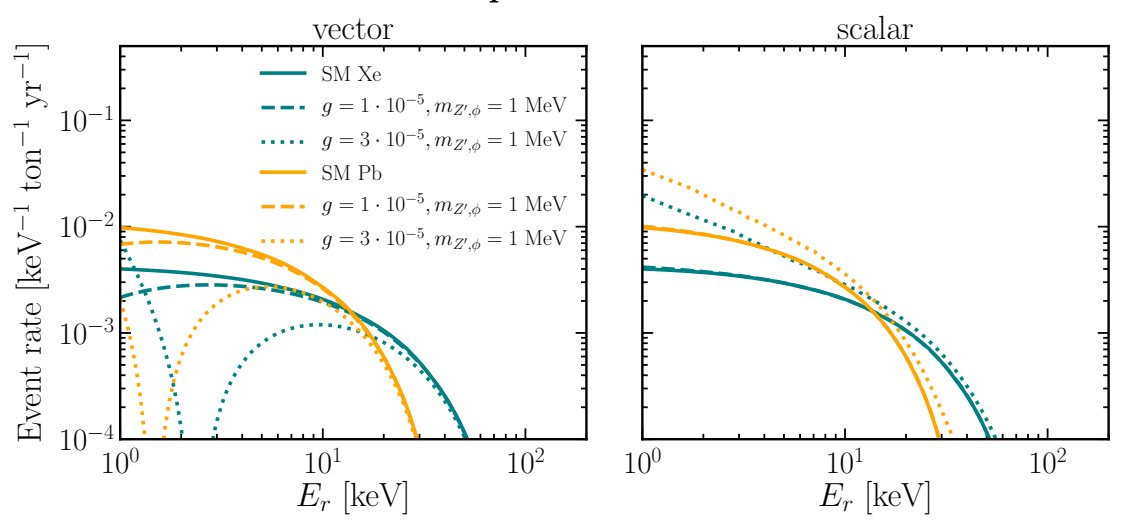


FIG. 5. Expected event rate as a function of the nuclear recoil energy induced by atmospheric neutrinos in Pb (orange) and Xe (blue) based detectors. The standard event rates (solid lines) are shown together with the ones involving non-standard coherent scattering on the left (right) for vector (scalar) mediators. Given the energy range of atmospheric neutrinos, the standard and non-standard rates are comparable for the vector and scalar scenarios.

VI. ATMOSPHERIC NEUTRINOS

Atmospheric neutrinos originate from the decay of mesons produced by the interactions of cosmic rays with nuclei in the Earth's atmosphere. The atmospheric neutrino flux at sub-GeV energies mainly consists of neutrinos from charged pion decays [52]. In the decay of a positively charged pion, a muon (anti)neutrino is created together with an electron neutrino:

$$\pi^+ \to \mu^+ + \nu_\mu \text{ and } \mu^+ \to e^+ + \bar{\nu}_\mu + \nu_e$$
. (20)

Similarly, for the negatively charged pion, two antineutrinos $\bar{\nu}_e$ and $\bar{\nu}_{\mu}$ and an electron neutrino are formed. Theoretical predictions on the low energy atmospheric neutrino are still plagued by high uncertainty ($\sim 20\%$) [85].

Future generation $\text{CE}\nu\text{NS}$ detectors will be able to observe the atmospheric neutrino background [52, 53]. We capitalize on this opportunity to explore how the presence of a non-standard coherent mediator could change the expected event rates. We rely on the inputs for the atmospheric neutrino flux provided in Ref. [52], where the atmospheric neutrino flux was calculated for the Gran Sasso location, where RES-NOVA and DARWIN will most likely be built.

Figure 5 shows the event rate induced by atmospheric neutrinos in Xe (green) and Pb based (orange) detectors. The expected number of events is reported for the standard (solid lines) and non-standard case (dashed and dotted lines). Differently from the solar event rate, but similarly to the SN rate, the Pb based detector is characterized by a higher number of events per ton at low recoil energies. Analogously to the SN and solar event rates, the new vector mediator can lead to a suppression or an

increase of the event rate; while, only an increase is possible in the scalar case (see Eqs. 5 and 10). Furthermore, by comparing the dashed lines with the ones from the solar neutrino event rate (Fig. 4), all being calculated for the same mass and mediator coupling, one can see that the difference between the standard and non-standard event rate is higher for a vector mediator, in the presence of relatively high energy neutrinos in the flux (closer or higher energy than $E_r^{\rm max}$ for which the form factor experiences a dip); this is due to the difference in the neutrino energy dependence of the non-standard cross section terms.

VII. DETECTOR CONSTRAINTS ON THE MASS AND COUPLING OF THE NEW MEDIATOR

In this section, we focus on deriving the perspective constraints on the $(g, m_{Z',\phi})$ parameter space for the new mediator by relying on SN, solar, and atmospheric neutrinos. In order to do that, we implement the χ^2 test using the pull method [86], with χ^2 defined as

$$\chi^2 = \min_{x} \sum_{\text{detector}} \left[\chi_{\text{detector}}^2 + \left(\frac{x}{\sigma_x}\right)^2 \right], \quad (21)$$

where σ_x is the flux normalization uncertainty. For each source and for each detector, $\chi^2_{\rm detector}$ is

$$\chi_{\text{detector}}^2 = -2 \ln \frac{L_0}{L_1} \ . \tag{22}$$

The likelihoods are given by

$$L_0 = \sum_{i} P(\lambda = N_{i,\nu N}; k = \overline{N}_{i,SM}) , \qquad (23)$$

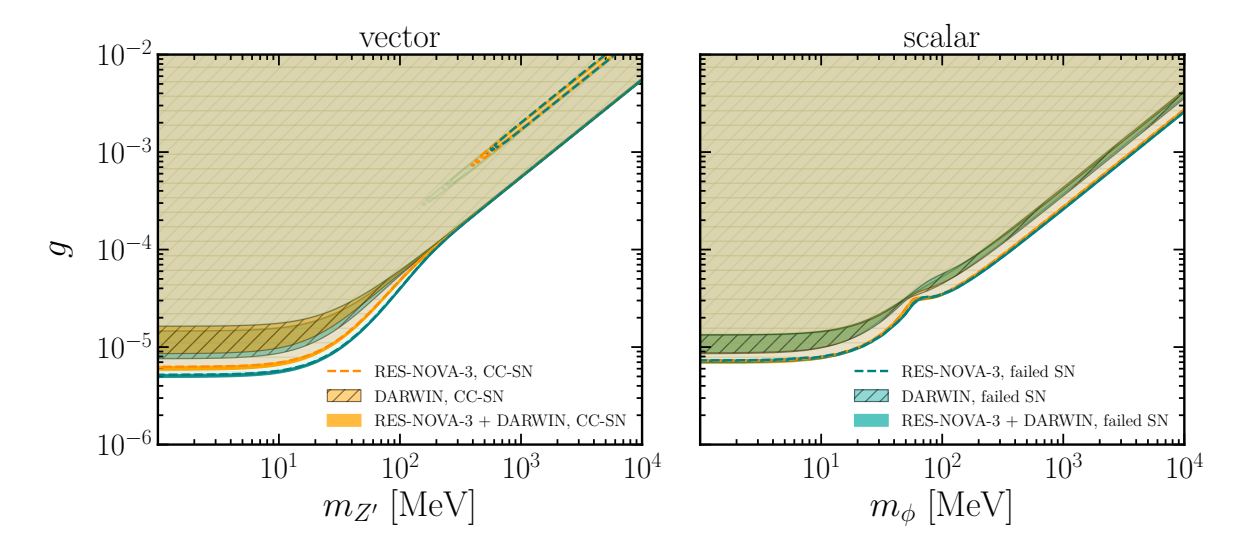


FIG. 6. Projected 90% CL sensitivity bounds on non-standard coherent scattering in the plane spanned by the mass $m_{Z',\phi}$ and coupling g of the new mediator. The vector (scalar) case is shown on the left (right) for a SN at 10 kpc from Earth. The sensitivity bounds for DARWIN (hatched regions), RES-NOVA-3 (dashed lines), and both detectors combined together (solid regions) are reported. The bounds for core-collapse SNe (CC-SN) are plotted in orange and the ones for the black hole forming collapses (failed SN) are in blue. The region of the parameter space excluded in the vector mediator scenario for low and intermediate mediator masses is bigger than the one excluded in the scalar case because of the more prominent energy dependent features induced by the vector mediator.

and

$$L_1 = \sum_{i} P(\lambda = \overline{N}_{i,SM}; k = \overline{N}_{i,SM}) ,$$
 (24)

where P is the Poisson distribution, i is the bin index and $\overline{N}_{i,\text{SM}}$ is the number of events observed in the i-th bin assuming the standard cross section only, whereas the number of the events when the new mediator is included is $N_{\nu N} = (1+x)\overline{N}_{\nu N}$ where $x \in (-1, \inf)$.

The statistical analysis has been developed by using a 2 keV binning [31, 53] of the event rates observed in RES-NOVA-3 and DARWIN. Additionally, the sensitivity bounds rely on a 100% efficiency for RES-NOVA and DARWIN; for the Xe based detector we also use the energy dependent efficiency of XENON1T [38, 64] for comparison; as such the excluded regions are defined by a finite band size instead than a curve.

A. Constraints from supernova neutrinos

By relying on the fact that the new mediator could enhance the coupling of SN neutrinos to matter in the stellar core and, therefore, modify the diffusion time of neutrinos, in Fig. 2 we show the region of the (g,m) parameter space disfavored by this argument. Additionally, as discussed in Sec. IV B, SN neutrinos can also undergo non-standard interactions in the detector.

The χ^2 test obtained by using the non-standard recoil rates shown in Fig. 3, provides the sensitivity bounds reported in Fig. 6 for a SN at 10 kpc, assuming a normalization uncertainty on the SN signal of 25%; this uncertainty

takes into account the early and late time maximal variation in the neutrino signal obtained by comparing different SN hydrodynamical simulations [87], the SN mass dependence [88], and the uncertainty in the SN distance determination [89, 90] (see Appendix A for more details).

The bounds in Fig. 6 are obtained for the non-standard vector (on the left) and scalar mediators (on the right) from a galactic SN burst detected in DARWIN (hatched regions), RES-NOVA-3 (dashed lines), and both detectors combined (solid regions). The bounds are shown for the core-collapse (orange) and failed SN cases (blue).

The shape of the excluded region is similar in the vector and scalar mediator scenarios. In the low mass limit, $m_{Z',\phi} \ll 2E_r m_T$, the change in the cross section is caused by g only; this results in no dependence of the excluded region on the new mediator mass below $\mathcal{O}(10)$ MeV. In the high mass region, $m_{Z',\phi} \ll 2E_r m_T$, the bounds depend on the effective coupling g^4/m_ϕ^4 for the scalar mediator and $g^2/m_{Z'}^2$ ($g^4/m_{Z'}^4$) for the vector mediator when the standard term is comparable to (or much smaller than) the non-standard one in Eq. 6. In addition, in the high mass limit for the vector mediator case, one can restore the standard cross section when the interference term $(-3Q_wAg^2/\sqrt{2}G_Fm_{Z'}^2)$ is comparable to the non-standard term in Eq. 6. This results in a small unconstrained island in the $(g, m_{Z'})$ plane (see Appendix B for more details on the event rate dependence on the mediator mass). Given that core-collapse SNe and black-hole-forming collapses exhibit a different neutrino signal, we report the exclusion bounds for both cases in Fig. 6.

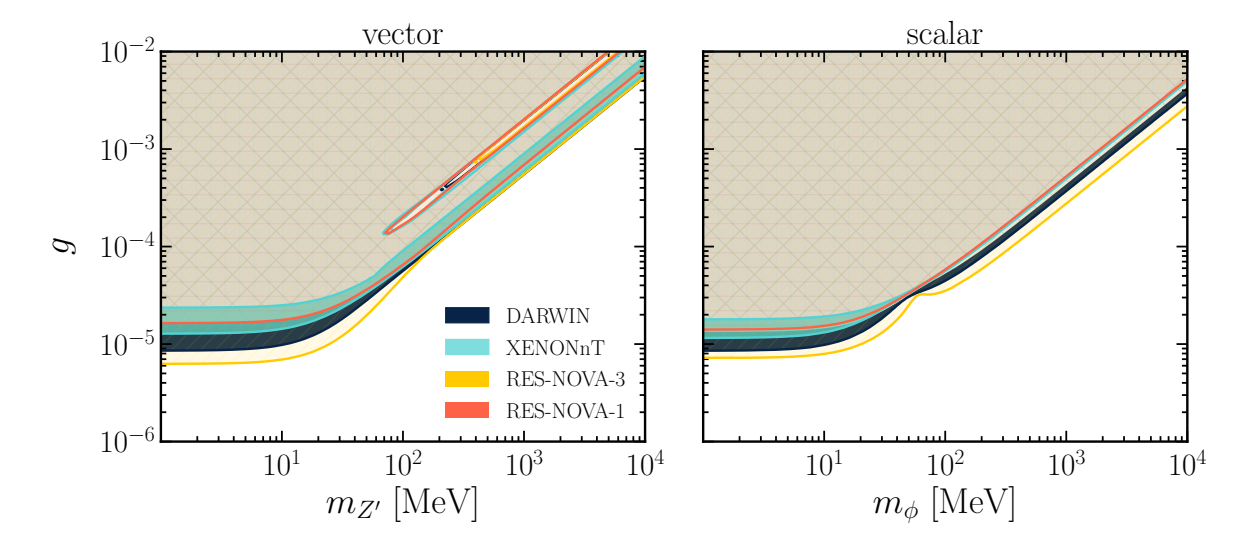


FIG. 7. Projected 90% CL sensitivity bounds on non-standard coherent scattering in the plane spanned by the mass $m_{Z',\phi}$ and coupling g of the new mediator. The vector (scalar) case is shown on the left (right) panel for a SN at 10 kpc from Earth. The bounds for DARWIN (navy-blue), XENONnT (cyan) RES-NOVA-3 (yellow) and RES-NOVA-1 (red) are shown, each marginalized over the core-collapse and failed SN models. The bounds are less stringent for smaller detectors.

Due to the smaller effective volume of the detector. and smaller event rate per ton (see Fig. 3), the DARWIN bounds are less stringent than the ones obtained from RES-NOVA-3, independently of the mediator type. The projected limits have a finite size uncertainty band for DARWIN because we use the 100% detector efficiency and the energy-dependent one. The efficiency band is wider in the low mass region as the shape of the recoil spectrum can be distinctly changed by the new mediator. The ruled-out region for the vector mediator in the low and intermediate mass region is bigger for the black hole forming collapse than for the core-collapse SN. This is due to the higher variability of the event rate shape (see Fig. 3) in that region than in the case of the large mediator mass, for which only the effective coupling matters; the latter only affects the normalization of the event rate, and the fact that the event rate extends to higher recoil energies due to the hotter spectra of neutrinos from black-hole-forming collapses does not matter anymore. This is not visible for the scalar mediator scenario as the rate can only increase with respect to the standard one.

Given the high event rate foreseen for SN neutrinos, we also explore the sensitivity limits for smaller detector volumes. In particular, we focus on RES-NOVA-1 (2.4 ton) [53], which should be operational within the next 2 years, and XENONnT (4 ton) [29]—whose tank is currently being filled with liquid Xe. For both detectors, we assume the same thresholds and efficiencies as for the RES-NOVA-3 and DARWIN. The results are reported in Fig. 7; the sensitivity increases with the effective volume of the detector, as expected. Despite the higher event rate per one ton of Pb (Fig. 3), the limits from RES-NOVA-1 are worse than the ones from XENONnT due to the smaller effective volume of the detector, unless the

XENONnT efficiency is worse than 100%. Note that, in this figure, as well as in Fig. 1, we report the combined bound obtained by marginalizing over the two different SN types (CC-SN and failed SN).

B. Constraints from solar and atmospheric neutrinos

As shown in Secs. V and VI, the recoil energy spectrum from solar and atmospheric neutrinos has characteristic signatures in the presence of non-standard coherent scattering. In the following, we assume that the 1σ normalization uncertainty for the atmospheric and solar neutrino fluxes is $\sigma_{\rm atm}=20\%$ [85] and $\sigma_{\rm sol}=10\%$ [91–93], respectively. Figure 8 shows the projected sensitivity bounds on the mass and coupling of the new mediator coming from the detection of solar and atmospheric neutrinos in DARWIN and RES-NOVA-3 for 1 yr exposure.

Figure 8 shows that the bounds from atmospheric neutrinos are less stringent than the ones from solar neutrinos. In fact, by comparing Figs. 4 and 5, one can see that the number of events induced by solar neutrinos is much larger than in the case of atmospheric neutrinos, despite the recoil spectra extending to higher energies for the latter. However, for the vector mediator (left panel), as the mediator mass increases, the bounds from solar neutrinos become slightly less competitive compared to the ones from atmospheric neutrinos. This is due to the possibility of experiencing energy dependent features over a larger recoil range than in the case of solar neutrinos. Nevertheless, due to the much smaller total number of events for atmospheric neutrinos, the solar bounds are always better. The solar neutrino bounds on the scalar

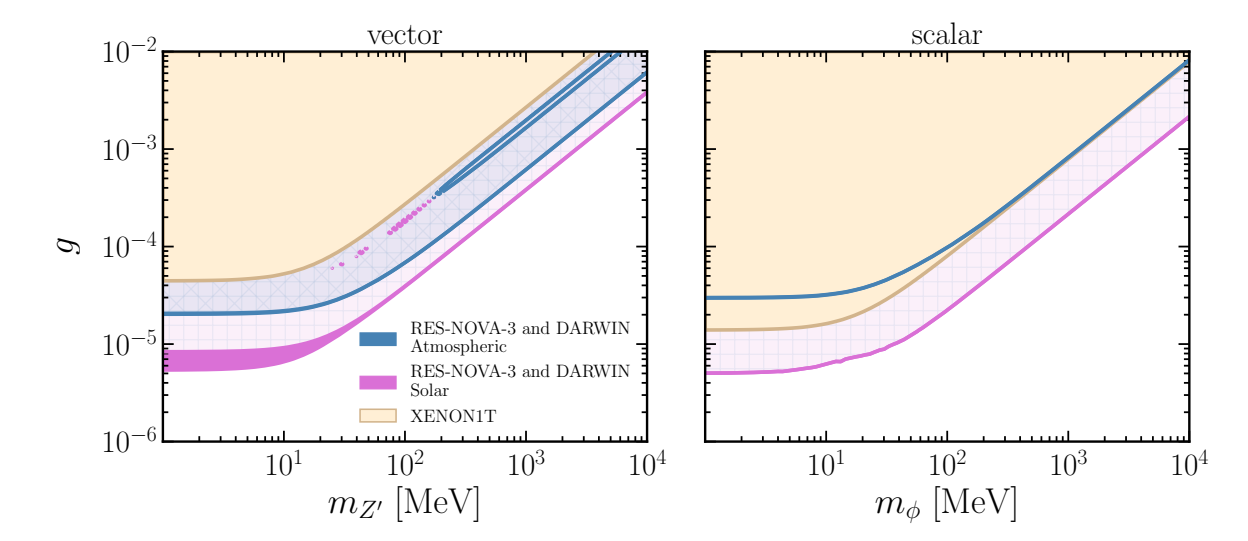


FIG. 8. Projected 90% CL sensitivity bounds on non-standard neutrino-nucleus interactions in the plane spanned by the mass and coupling of the new mediator. The vector (scalar) case is shown on the left (right). The bounds for the atmospheric neutrino signal are plotted in blue and for solar neutrinos in pink. The sensitivity bounds have been derived by relying on the detection of solar and atmospheric neutrinos in RES-NOVA-3 and DARWIN for 1 yr exposure. In addition, the bounds obtained using the XENON1T limits on WIMPs [38] are also shown in beige. Due to the much higher even rate of solar neutrinos, the solar bounds are more stringent than the ones coming from atmospheric neutrinos.

mediator are better than the ones on the vector mediator, and the opposite effect is true for atmospheric neutrinos. This is due to the fact that atmospheric neutrinos have much higher energies than solar neutrinos, and the non-standard cross section for the scalar mediator is smaller than the one for the vector mediator case in the high-energy neutrino limit (see Sec. VI). Since the volume of RES-NOVA-3 is expect to be 10 times larger than the one of DARWIN, there is no uncertainty band connected to the different efficiencies used to calculate the bounds except for the solar neutrino vector case, where the Xe based detector probes twice the energy range than the Pb one. This is not evident for the scalar case due to the insensitivity of the low mediator mass cross section to the target material (see Sec. V).

Our projected 90%CL sensitivity for solar neutrinos in RES-NOVA-3 and DARWIN in the vector mediator case is in good agreement with the one in Ref. [13], where the authors calculated the bounds for the Xe based detector using 200 ton-yrs exposure, 100% detector efficiency, 1 keV energy threshold, and zero background. However, the 200 ton yrs exposure in [13] is obtained by using the DARWIN volume integrated over 5 yrs, while we consider 1 yr only. The reduced exposure time makes our results a bit less competitive than the ones reported in Ref. [13], despite the fact that we combine RES-NOVA-3 and DARWIN. Our bounds are in fact completely driven by the Xe based detector that performs better in the energy range of solar neutrinos and are not improved much by the addition of RES-NOVA-3.

Additionally, we estimate the current 90% CL upper constraints on the mass and coupling of the new medi-

ator of non-standard neutrino-nucleus interactions from the XENON1T data [38], assuming the current detector threshold (0.7 keV) and efficiency for the S2 channel. In order to do that, we estimate the maximal event rate per 1 year of XENON1T exposure by taking the upper bound coming from calculating the event rates for the correspondent bounds on the WIMP masses and spin independent cross sections through the WIMPrates package [94], under the assumption of a standard isothermal dark matter halo [38, 64]. The resultant bounds for vector and scalar mediators are presented in Fig. 8. Similarly to the bounds obtained by looking at the diffusion time for SN neutrinos, the bounds for the scalar mediator are more stringent.

VIII. DISCUSSION AND CONCLUSIONS

We employ astrophysical neutrinos to constrain non-standard coherent neutrino-nucleus scattering for vector and scalar mediators, as summarized in Fig. 1. In particular, we rely on the impact that the non-standard coherent neutrino-nucleus scattering would have on the physics of core-collapse supernovae, as well as the effect of non-standard reactions occurring between supernova, solar and atmospheric neutrinos and the nuclei in RES-NOVA, DARWIN, XENONnT, and XENON1T.

If non-standard coherent neutrino-nucleus scattering should occur in the supernova core, neutrinos would need more time to diffuse out, with possible implications on the supernova explosion mechanism. In addition, for the lepton number conserving interactions mediated by a scalar particle, we have also calculated the limits on the mass and coupling of the mediator using the cooling criterion [76]. The bounds derived through these arguments fall in the region of the parameter space constrained by COHERENT [23], SuperCDMS, CDMSlite, LUX [13].

In order to derive bounds on non-standard coherent neutrino-nucleus scattering in upcoming $\text{CE}\nu\text{NS}$ detectors, we focus on the fact that the nuclear recoil spectrum changes its shape and normalization in the presence of a new vector or scalar mediator.

We have shown that the observation of the neutrino signal from a galactic supernova in DARWIN and RESNOVA can potentially place the most stringent constraints. The improvement on current bounds from COHERENT [23] is up to 50% in the limit of low mediator masses. Recently Ref. [95] highlighted the possibility of reducing the energy threshold in dual phase xenon detectors to 0.3 keV. In this case, our bounds would improve significantly (up to $\sim 50\%$).

The sensitivity projections for solar and atmospheric neutrinos show that solar neutrinos will be driving the bounds on the non-standard mediator because of the larger event rate with respect to atmospheric neutrinos. In particular, 1 yr exposure to solar neutrinos could exclude a region of the parameter space similar to the one excluded by the observation of neutrinos from a galactic supernova burst. However, DARWIN will be more competitive on the solar neutrino bounds, given its better performance in the energy range of interest; while the supernova neutrino bounds will be driven by RES-NOVA-3 because of the higher energies of supernova neutrinos that are responsible for a higher event rate in lead.

Our results indicate that detectors employing lead and xenon targets are characterized by comparable sensitivity to non-standard interactions, given akin volumes. It is, however, important to notice that while the detection of solar and atmospheric neutrinos is connected to overcoming detector backgrounds, the observation of supernova neutrinos is essentially background free, thanks to the transient nature of the signal and the high expected event rate, at the price of being a rare event. We have also tested the sensitivity of XENON1T to non-standard coherent scattering between neutrinos and nuclei. XENON1T performs better than LUX [13, 56], due to its bigger effective volume, but the bounds obtained by COHERENT [23] are more stringent.

In conclusion, the possibility of detecting astrophysical neutrinos with coherent neutrino-nucleus scattering detectors opens a new window to explore New Physics. Excitingly, it also promises to place the most competitive bounds on non-standard neutrino-nucleus coherent scattering.

ACKNOWLEDGMENTS

We are grateful to Patrick Decowski, Rafael Lang, and Shashank Shalgar for helpful discussions and Diego Aristizabal Sierra for feedback on the manuscript. We also thank Robert Bollig, Thomas Ertl, and Thomas Janka for granting access to the data of the supernova models adopted in this work. This work was supported by the Villum Foundation (Project No. 13164), the Carlsberg Foundation (CF18-0183), the Knud Højgaard Foundation, the Deutsche Forschungsgemeinschaft through Sonderforschungbereich SFB 1258 "Neutrinos and Dark Matter in Astro- and Particle Physics" (NDM).

Appendix A: Impact of the uncertainty in the supernova model, mass and distance

To test the impact of the uncertainty in resolving the SN distance, and the possible uncertainty in the SN neutrino signal (expressed as an uncertainty on the signal normalization), we compute the projected 90% CL exclusion regions for a SN at 10 kpc from Earth, assuming 10% and 25% uncertainty on the flux normalization. This normalization band includes uncertainties in determining the SN distance [89, 90], differences in the neutrino properties from various one-dimensional hydrodynamical SN simulations [87], and uncertainties on the dependence of the neutrino emission properties from the SN mass [88].

Figure 9 shows the calculated bounds. The solid regions show results obtained by adopting the SN neutrino signal with a normalization uncertainty of 25% and the dashed ones refer to the 10% normalization uncertainty. Additionally, in order to take into account differences between the CC-SN and failed SN models (different shapes of the time integrated SN flux), the bounds are marginalized over the CC-SN and failed SN models. The left panel of Fig. 9 illustrates the expected bounds for the vector mediator case; the higher normalization uncertainty only affects the high mass part of the contour plot. This is explained by the absence of event rate features for high masses of the vector mediator and the simple $(g^4/m_{Z'}^2)$ or $(g^4/m_{Z'}^4)$ effective coupling, which affect the normalization of the resulting recoil rate. For the scalar mediator case (plot on the right of Fig. 9), because of the different kinetic term between the scalar cross section and the vector one, the change of the normalization uncertainty does not affect the projected constraints significantly, see also Appendix B.

Appendix B: Dependence of the supernova neutrino rate on the mediator mass

To better understand the shape of the exclusion bounds for the vector and scalar mediators in Figs. 6–8, we here focus on the spectral features of the predicted recoil rates in three different mass regimes. Figure 10 illustrates the event rates for a galactic supernova (CC-NS) at 10 kpc from Earth in a Xe based detector. The rates for the vector (scalar) mediator are in the top (bottom) panels. In each plot, the solid blue lines represent

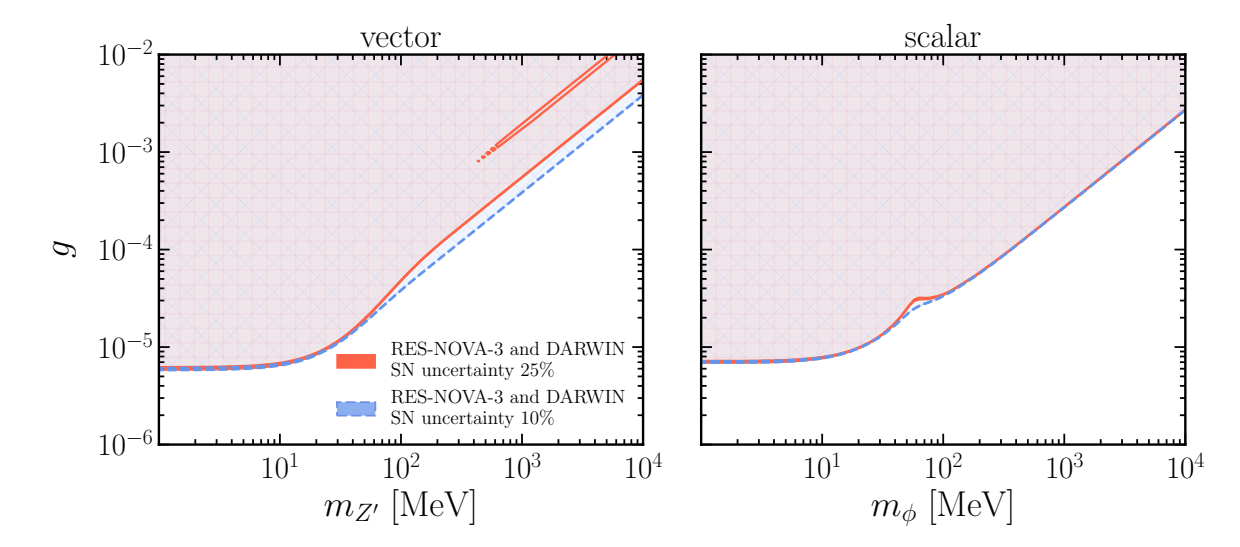


FIG. 9. Projected 90% CL sensitivity bounds on the mass and coupling of the new vector (on the left) and scalar (on the right) mediators for a SN burst at 10 kpc from Earth detected in RES-NOVA-3 and DARWIN. The plotted bounds are marginalized over CC- and failed SNe. The solid (dashed) lines represent the bounds for the 1σ normalization uncertainty equal to 25% (10%). The 10% uncertainty significantly helps only for the case of high mass vector mediator.

the event rate for the standard cross section and the orange band represents its 25% normalization uncertainty. The event rates in the presence of the new mediator are plotted as blue and beige lines for the same mediator mass and coupling, respectively. From Fig. 10, we see that the event rates for the scalar mediator are always larger than the standard recoil rate.

In the low mediator mass limit $(2E_r m_T >> m_{\{Z',\phi\}}^2)$, left panels of Fig. 10) the event rates are insensitive to the mass of the mediator independently of the mediator type. The recoil spectra for the intermediate mediator mass region $(2E_r m_T \sim m_{\{Z',\phi\}}^2)$, middle panels in Fig. 10) are sensitive to both mass and coupling of the mediator. In the low and medium mass regime (left and middle panels of Fig. 10), the event rates for the new vector mediator experience characteristic dips in the recoil spectrum due to the presence of the interference term between the standard and non-standard terms in Eq. 5.

The exact location of the dip depends on the new mediator coupling [23]:

$$E_r = \frac{2g_{\nu,Z'}Q_w' - \sqrt{2}G_F m_{Z'}Q_w}{2\sqrt{2}G_F Q_w m_T} .$$
 (B1)

In the high mediator mass limit $(2E_r m_T << m_{\{Z',\phi\}}^2)$, right panels in Fig. 10), the non-standard couplings become effective couplings. For the vector mediator, the effective coupling is $\sim g^4/m_{Z'}^2$ when the interference term dominates and $\sim g^4/m_{Z'}^2$ when the non-standard term dominates. This effectively means that the total cross section (Eq. 5) has the same energy dependence as the standard one, but another normalization. For the scalar mediator case, since there is no interference term, the non-standard part of the total cross section (Eq. 10) will scale as $\sim g^4/m_\phi^4$. However, due to the different kinematic term with respect to the standard term, the new total cross section cannot be simply obtained by varying the cross section normalization.

D. Z. Freedman, Phys. Rev. D 9, 1389 (1974).

^[2] D. Akimov et al. (COHERENT), Science 357, 1123 (2017), arXiv:1708.01294 [nucl-ex].

^[3] D. Akimov et al. (COHERENT), (2018), 10.5281/zenodo.1228631, arXiv:1804.09459 [nucl-ex].

^[4] K. Scholberg, Phys. Rev. D 73, 033005 (2006), arXiv:hepex/0511042.

^[5] A. Dodd, E. Papageorgiu, and S. Ranfone, Phys. Lett. B 266, 434 (1991).

^[6] J. Barranco, O. Miranda, and T. Rashba, JHEP 12, 021 (2005), arXiv:hep-ph/0508299.

^[7] J. Barranco, O. Miranda, and T. Rashba, Phys. Rev. D 76, 073008 (2007), arXiv:hep-ph/0702175.

^[8] A. Anderson, J. Conrad, E. Figueroa-Feliciano, C. Ignarra, G. Karagiorgi, K. Scholberg, M. Shaevitz, and J. Spitz, Phys. Rev. D 86, 013004 (2012), arXiv:1201.3805 [hep-ph].

^[9] T. Kosmas, O. Miranda, D. Papoulias, M. Tortola, and J. Valle, Phys. Rev. D 92, 013011 (2015), arXiv:1505.03202 [hep-ph].

^[10] B. Dutta, R. Mahapatra, L. E. Strigari, and J. W. Walker, Phys. Rev. D 93, 013015 (2016),

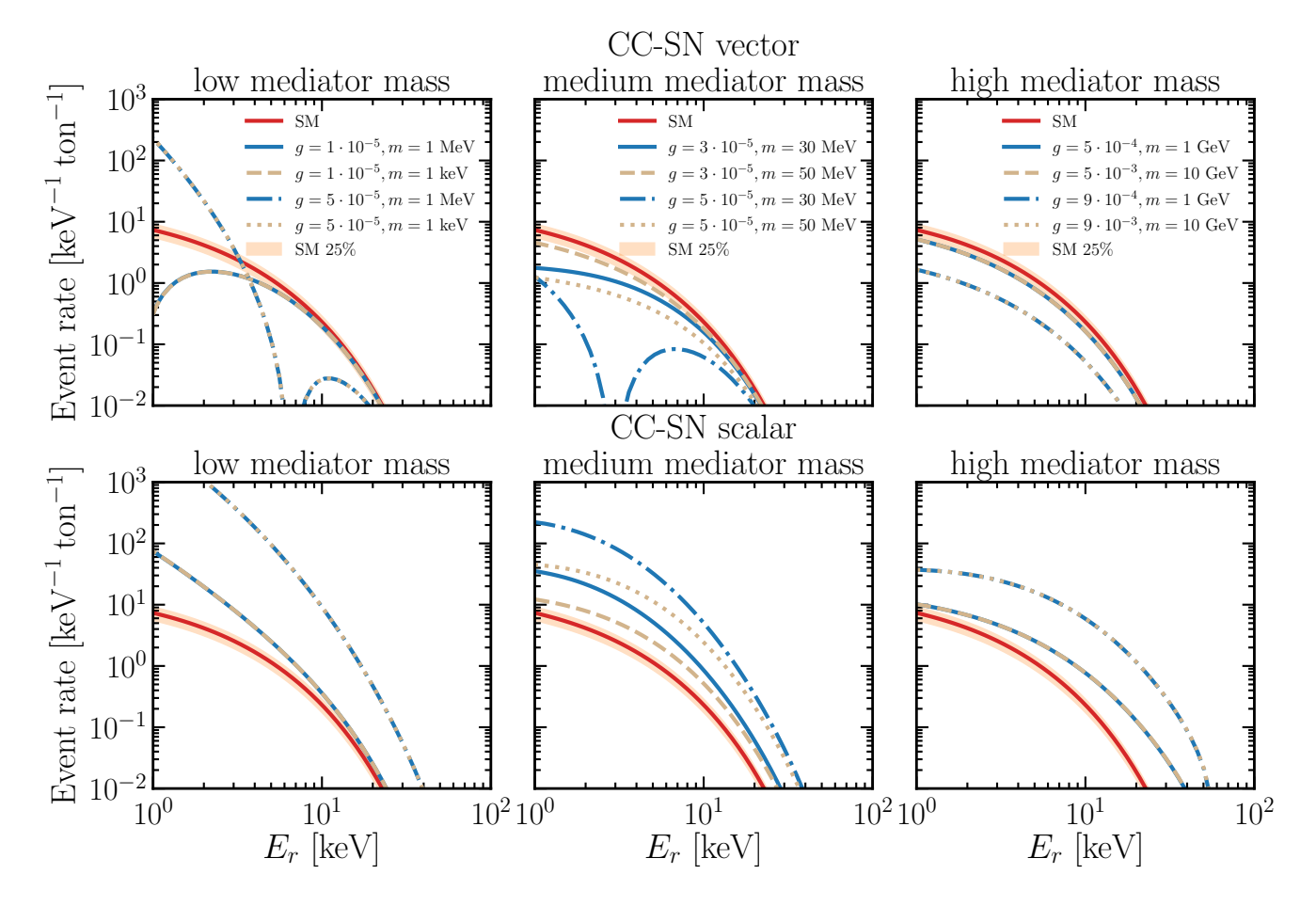


FIG. 10. Expected event rate as a function of the nuclear recoil energy induced by the neutrino signal from a galactic supernova (CC-SN) at 10 kpc per 1 ton of Xe detector for vector and scalar mediators are shown in blue and beige, in the top and bottom panels, respectively. The standard event rate (solid red lines) and its 25% normalization uncertainty (orange band) is plotted for reference. The event rate in the case of low, medium and high mediator masses is plotted in the left, middle and right panels respectively. In the case of a new scalar mediator, the rate always results in higher recoil rates than in the standard scenario; this is not the case for the vector mediator scenario.

- arXiv:1508.07981 [hep-ph].
- [11] B. Dutta, Y. Gao, R. Mahapatra, N. Mirabolfathi, L. E. Strigari, and J. W. Walker, Phys. Rev. D 94, 093002 (2016), arXiv:1511.02834 [hep-ph].
- [12] M. Lindner, W. Rodejohann, and X.-J. Xu, JHEP 03, 097 (2017), arXiv:1612.04150 [hep-ph].
- [13] D. G. Cerdeño, M. Fairbairn, T. Jubb, P. A. N. Machado, A. C. Vincent, and C. Bæhm, JHEP 05, 118 (2016), [Erratum: JHEP 09, 048 (2016)], arXiv:1604.01025 [hep-ph].
- [14] J. B. Dent, B. Dutta, S. Liao, J. L. Newstead, L. E. Strigari, and J. W. Walker, Phys. Rev. D 96, 095007 (2017), arXiv:1612.06350 [hep-ph].
- [15] J. Liao and D. Marfatia, Phys. Lett. B 775, 54 (2017), arXiv:1708.04255 [hep-ph].
- [16] P. Coloma, M. Gonzalez-Garcia, M. Maltoni, and T. Schwetz, Phys. Rev. D 96, 115007 (2017), arXiv:1708.02899 [hep-ph].
- [17] P. Coloma, P. B. Denton, M. Gonzalez-Garcia, M. Maltoni, and T. Schwetz, JHEP 04, 116 (2017), arXiv:1701.04828 [hep-ph].
- [18] D. Papoulias and T. Kosmas, Phys. Rev. D 97, 033003

- (2018), arXiv:1711.09773 [hep-ph].
- [19] I. M. Shoemaker, Phys. Rev. D 95, 115028 (2017), arXiv:1703.05774 [hep-ph].
- [20] J. B. Dent, B. Dutta, S. Liao, J. L. Newstead, L. E. Strigari, and J. W. Walker, Phys. Rev. D 97, 035009 (2018), arXiv:1711.03521 [hep-ph].
- [21] Y. Farzan, M. Lindner, W. Rodejohann, and X.-J. Xu, JHEP 05, 066 (2018), arXiv:1802.05171 [hep-ph].
- [22] P. B. Denton, Y. Farzan, and I. M. Shoemaker, JHEP 07, 037 (2018), arXiv:1804.03660 [hep-ph].
- [23] D. Aristizabal Sierra, B. Dutta, S. Liao, and L. E. Stri-gari, JHEP 12, 124 (2019), arXiv:1910.12437 [hep-ph].
- [24] M. Cadeddu, N. Cargioli, F. Dordei, C. Giunti, Y. Li, E. Picciau, and Y. Zhang, (2020), arXiv:2008.05022 [hep-ph].
- [25] P. B. Denton and J. Gehrlein, (2020), arXiv:2008.06062 [hep-ph].
- [26] E. Aprile et al. (XENON), JCAP 04, 027 (2016), arXiv:1512.07501 [physics.ins-det].
- [27] D. Akerib *et al.* (LUX), Phys. Rev. Lett. **118**, 021303 (2017), arXiv:1608.07648 [astro-ph.CO].
- [28] K. Abe et al. (XMASS), Phys. Lett. B **789**, 45 (2019),

- arXiv:1804.02180 [astro-ph.CO].
- [29] E. Aprile et al. (XENON), (2020), arXiv:2007.08796 [physics.ins-det].
- [30] D. Akerib et al. (LZ), (2015), arXiv:1509.02910 [physics.ins-det].
- [31] J. Aalbers et al. (DARWIN), JCAP 11, 017 (2016), arXiv:1606.07001 [astro-ph.IM].
- [32] D. Z. Freedman, D. N. Schramm, and D. L. Tubbs, Ann. Rev. Nucl. Part. Sci. 27, 167 (1977).
- [33] A. Drukier and L. Stodolsky, Phys. Rev. D , 395 (1984).
- [34] J. F. Beacom, W. M. Farr, and P. Vogel, Phys. Rev. D 66, 033001 (2002), arXiv:hep-ph/0205220.
- [35] C. J. Horowitz, K. Coakley, and D. McKinsey, Phys. Rev. D 68, 023005 (2003), arXiv:astro-ph/0302071.
- [36] K. Scholberg, Ann. Rev. Nucl. Part. Sci. 62, 81 (2012), arXiv:1205.6003 [astro-ph.IM].
- [37] A. Nikrant, R. Laha, and S. Horiuchi, Phys. Rev. D 97, 023019 (2018), arXiv:1711.00008 [astro-ph.HE].
- [38] E. Aprile et al. (XENON), Phys. Rev. Lett. 123, 251801 (2019), arXiv:1907.11485 [hep-ex].
- [39] R. F. Lang, C. McCabe, S. Reichard, M. Selvi, and I. Tamborra, Phys. Rev. D 94, 103009 (2016), arXiv:1606.09243 [astro-ph.HE].
- [40] T. Marrodán Undagoitia and L. Rauch, J. Phys. G 43, 013001 (2016), arXiv:1509.08767 [physics.ins-det].
- [41] N. Raj, V. Takhistov, and S. J. Witte, Phys. Rev. D 101, 043008 (2020), arXiv:1905.09283 [hep-ph].
- [42] N. Raj, Phys. Rev. Lett. 124, 141802 (2020), arXiv:1907.05533 [hep-ph].
- [43] D. Khaitan (LZ), JINST 13, C02024 (2018), arXiv:1801.05651.
- [44] K. Abe et al. (XMASS), Astropart. Phys. 89, 51 (2017), arXiv:1604.01218 [physics.ins-det].
- [45] T. Kozynets, S. Fallows, and C. B. Krauss, Astropart. Phys. 105, 25 (2019), arXiv:1806.01417 [astro-ph.HE].
- [46] J. Vergados and H. Ejiri, Nucl. Phys. B 804, 144 (2008), arXiv:0805.2583 [hep-ph].
- [47] J. Billard, L. Strigari, and E. Figueroa-Feliciano, Phys. Rev. D 89, 023524 (2014), arXiv:1307.5458 [hep-ph].
- [48] C. Bœhm, D. Cerdeño, P. Machado, A. Olivares-Del Campo, E. Perdomo, and E. Reid, JCAP 01, 043 (2019), arXiv:1809.06385 [hep-ph].
- [49] J. Billard, L. E. Strigari, and E. Figueroa-Feliciano, Phys. Rev. D 91, 095023 (2015), arXiv:1409.0050 [astro-ph.CO].
- [50] R. Budnik, O. Chesnovsky, O. Slone, and T. Volansky, Phys. Lett. B 782, 242 (2018), arXiv:1705.03016 [hep-ph]
- [51] J. L. Newstead, L. E. Strigari, and R. F. Lang, Phys. Rev. D 99, 043006 (2019), arXiv:1807.07169 [astro-ph.SR].
- [52] J. L. Newstead, R. F. Lang, and L. E. Strigari, (2020), arXiv:2002.08566 [astro-ph.CO].
- [53] L. Pattavina, N. Ferreiro Iachellini, and I. Tamborra, Phys. Rev. D 102, 063001 (2020), arXiv:2004.06936 [astro-ph.HE].
- [54] R. Agnese et al. (SuperCDMS), Phys. Rev. Lett. 116, 071301 (2016), arXiv:1509.02448 [astro-ph.CO].
- [55] R. Agnese et al. (SuperCDMS), Phys. Rev. Lett. 112, 241302 (2014), arXiv:1402.7137 [hep-ex].
- [56] D. Akerib *et al.* (LUX), Phys. Rev. Lett. **116**, 161301 (2016), arXiv:1512.03506 [astro-ph.CO].
- [57] J. Hakenmüller et al., Eur. Phys. J. C 79, 699 (2019), arXiv:1903.09269 [physics.ins-det].

- [58] R. Strauss et al., Eur. Phys. J. C 77, 506 (2017), arXiv:1704.04320 [physics.ins-det].
- [59] A. Aguilar-Arevalo et al. (CONNIE), Phys. Rev. D 100, 092005 (2019), arXiv:1906.02200 [physics.ins-det].
- [60] G. Agnolet et al. (MINER), Nucl. Instrum. Meth. A 853, 53 (2017), arXiv:1609.02066 [physics.ins-det].
- [61] D. Akimov et al. (RED), JINST 8, P10023 (2013), arXiv:1212.1938 [physics.ins-det].
- [62] C. Patrignani et al. (Particle Data Group), Chin. Phys. C 40, 100001 (2016).
- [63] R. H. Helm, Phys. Rev. 104, 1466 (1956).
- [64] E. Aprile et al. (XENON), Phys. Rev. Lett. 121, 111302 (2018), arXiv:1805.12562 [astro-ph.CO].
- [65] E. Vitagliano, I. Tamborra, and G. G. Raffelt, (2019), arXiv:1910.11878 [astro-ph.HE].
- [66] A. Mirizzi, I. Tamborra, H.-T. Janka, N. Saviano, K. Scholberg, R. Bollig, L. Hüdepohl, and S. Chakraborty, Riv. Nuovo Cim. 39, 1 (2016), arXiv:1508.00785 [astro-ph.HE].
- [67] H. A. Bethe and J. R. Wilson, Astrophys. J. 295, 14 (1985).
- [68] A. Strumia and F. Vissani, Phys. Lett. B 564, 42 (2003), arXiv:astro-ph/0302055.
- [69] C. Giunti and C. W. Kim, Fundamentals of Neutrino Physics and Astrophysics (Oxford University Press, 2007).
- [70] "Garching core-collapse supernova archive," https://wwwmpa.mpa-garching.mpg.de/ccsnarchive/.
- [71] A. W. Steiner, M. Hempel, and T. Fischer, Astrophys. J. 774, 17 (2013), arXiv:1207.2184 [astro-ph.SR].
- [72] K. Hirata *et al.* (Kamiokande-II), Phys. Rev. Lett. 58, 1490 (1987).
- [73] R. Bionta et al., Phys. Rev. Lett. 58, 1494 (1987).
- [74] S. Chakraborty, R. Hansen, I. Izaguirre, and G. G. Raffelt, Nucl. Phys. B 908, 366 (2016), arXiv:1602.02766 [hep-ph].
- [75] S. Chandrasekhar, Rev. Mod. Phys. 15, 1 (1943).
- [76] G. G. Raffelt, Stars as Laboratories for Fundamental Physics (Chicago University Press, USA, 1996).
- [77] T. Sukhbold, T. Ertl, S. Woosley, J. M. Brown, and H. T. Janka, Astrophys. J. 821, 38 (2016), arXiv:1510.04643 [astro-ph.HE].
- [78] C. Basinger, C. Kochanek, S. Adams, X. Dai, and K. Stanek, (2020), arXiv:2007.15658 [astro-ph.SR].
- [79] M. T. Keil, G. G. Raffelt, and H.-T. Janka, Astrophys. J. 590, 971 (2003), arXiv:astro-ph/0208035.
- [80] I. Tamborra, B. Müller, L. Hüdepohl, H.-T. Janka, and G. G. Raffelt, Phys. Rev. D 86, 125031 (2012), arXiv:1211.3920 [astro-ph.SR].
- [81] R. Harnik, J. Kopp, and P. A. Machado, JCAP 07, 026 (2012), arXiv:1202.6073 [hep-ph].
- [82] B. Dutta, S. Liao, L. E. Strigari, and J. W. Walker, Phys. Lett. B 773, 242 (2017), arXiv:1705.00661 [hep-ph].
- [83] D. Aristizabal Sierra, N. Rojas, and M. Tytgat, JHEP 03, 197 (2018), arXiv:1712.09667 [hep-ph].
- [84] M. Gonzalez-Garcia, M. Maltoni, Y. F. Perez-Gonzalez, and R. Zukanovich Funchal, JHEP 07, 019 (2018), arXiv:1803.03650 [hep-ph].
- [85] M. Honda, T. Kajita, K. Kasahara, and S. Midorikawa, Phys. Rev. D 83, 123001 (2011), arXiv:1102.2688 [astro-ph.HE].
- [86] G. Fogli, E. Lisi, A. Marrone, D. Montanino, and A. Palazzo, Phys. Rev. D 66, 053010 (2002), arXiv:hepph/0206162.

- [87] E. O'Connor et al., J. Phys. G 45, 104001 (2018), arXiv:1806.04175 [astro-ph.HE].
- [88] S. Seadrow, A. Burrows, D. Vartanyan, D. Radice, and M. A. Skinner, Mon. Not. Roy. Astron. Soc. 480, 4710 (2018), arXiv:1804.00689 [astro-ph.HE].
- [89] M. Kachelrieß, R. Tomás, R. Buras, H.-T. Janka, A. Marek, and M. Rampp, Phys. Rev. D 71, 063003 (2005), arXiv:astro-ph/0412082.
- [90] S. M. Adams, C. Kochanek, J. F. Beacom, M. R. Vagins, and K. Stanek, Astrophys. J. 778, 164 (2013), arXiv:1306.0559 [astro-ph.HE].
- [91] G. Bellini et al. (Borexino), Phys. Rev. D 82, 033006 (2010), arXiv:0808.2868 [astro-ph].
- [92] K. Abe *et al.* (Super-Kamiokande), Phys. Rev. D $\bf 94$, 052010 (2016), arXiv:1606.07538 [hep-ex].
- [93] M. Anderson et al. (SNO+), Phys. Rev. D 99, 012012 (2019), arXiv:1812.03355 [hep-ex].
- [94] J. Aalbers, B. Pelssers, and K. D. Morå, "Wimprates: v0.3.1," (2019).
- [95] B. Lenardo et al., (2019), arXiv:1908.00518 [physics.insdet].